Article

Not peer-reviewed version

# Titanium dioxide nanoparticle-imbedded polyelectrolyte multilayer as an osteoconductive and antimicrobial surface coating

Matthew Rothpan , Nitin Chandra Teja Dadi , Geoffrey McKay , Michael Tanzer , Dao Nguyen , Adam Hart * , Maryam Tabrizian *

Posted Date: 9 October 2023

doi: 10.20944/preprints202310.0493.v1

Keywords: Titanium dioxide nanoparticles; Silver nanoparticles; Polyelectrolyte; Layer by layer; Anti-biofilm coating; Bioactive coating; Orthopedic implants.

*Article*

# Titanium Dioxide Nanoparticle-Imbedded Polyelectrolyte Multilayer as an Osteoconductive and Antimicrobial Surface Coating

**Matthew Rothpan [1], Nitin Chandra Teja Dadi [2], Geoffrey Mckay [3], Michael Tanzer [2], Dao Nguyen [3,4,5], Adam Hart [2,*] and Maryam Tabrizian [1,6,*]**

[1] Department of Biomedical Engineering, Faculty of Medicine and Health Sciences, McGill University, Montreal, QC H3A 2B6, Canada
[2] Jo Miller Orthopaedic Research Laboratory, Division of Orthopaedic Surgery, McGill University, Montreal, QC H3G 1A4, Canada
[3] Meakins-Christie Laboratories, Research Institute of the McGill University Health Centre, Montreal, QCH4A 3J1, Canada
[4] Department of Microbiology and Immunology, McGill University, Montreal, QC H3A OG4, Canada;
[5] Department of Medicine, McGill University, Montreal, QC H4A 3J1, Canada
[6] Faculty of Dentistry and Oral Health Sciences, McGill University, 3640 Rue University, Montreal, QC H3A 0C7, Canada
* Correspondence: maryam.tabrizian@mcgill.ca; adam.hart@mcgill.ca

**Abstract:** Bioactive surface coatings have retained the attention of researchers and physicians due to their versatility and range of applications in orthopedics, particularly in infection prevention. Antibacterial metal nanoparticles (mNPs) are a promising therapeutic, with vast application opportunities on orthopedic implants. The current research aimed to construct a polyelectrolyte multilayer on a highly porous titanium implant using alternating thin film coatings of chitosan and alginate via the layer-by-layer (LbL) self-assembly technique, along with the incorporation of silver nanoparticles (AgNPs) or titanium dioxide nanoparticles ($TiO_2$NPs), for antibacterial and osteoconductive activity. These mNPs were characterized for their physicochemical properties using quartz crystal microgravimetry with dissipation system, nanoparticle tracking analysis, scanning electron microscopy, and atomic force microscopy. Their cytotoxicity and osteogenic differentiation capabilities were assessed by AlamarBlue and alkaline phosphatase (ALP) activity assays, respectively. The antibiofilm efficacy of the mNPs tested against *Staphylococcus aureus*. The LbL polyelectrolyte coating was successfully applied to the porous titanium substrate. A dose-dependent relationship between nanoparticle concentration and ALP as well as antibacterial effects was observed. $TiO_2$NP samples were also less cytotoxic than AgNP counterparts, although similarly antimicrobial. Together, these data serve as a proof-of-concept for a novel coating approach for orthopedic implants with antimicrobial and osteoconductive properties.

**Keywords:** titanium dioxide nanoparticles; silver nanoparticles; polyelectrolyte; layer by layer; anti-biofilm coating; bioactive coating; orthopedic implants

## 1. Introduction

Hip and knee replacements cost Canada $1.3 billion and were performed on 1.3 million people in 2020-2021 [1]. Treatment requires multiple surgeries, wound debridement, and implant removal. Prolonged intravenous antibiotic therapy is also required. However, infection eradication rates are only 83-87% [2]. Patients with Periprosthetic Joint Infection (PJI) have longer hospital stays, higher costs, and more time in the operating room. This results in an annual cost of over $42 million and 25,349 days of hospitalization. In the U. S. A, hospital expenses for PJI would reach $1.85 billion dollars by 2030 for hip and knee procedures [3]. PJI are increasingly problematic due to the growing of the antimicrobial resistance in the microorganisms that are primarily responsible for implant failure following the joint replacement surgery (Figure 1) [4–8].

Preprints (www.preprints.org) | NOT PEER-REVIEWED | Posted: 9 October 2023 doi:10.20944/preprints202310.0493.v1



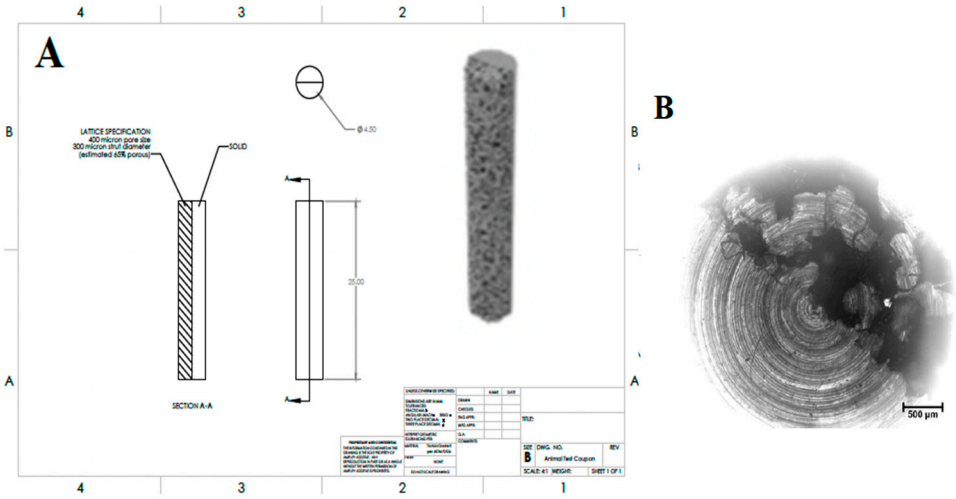


**Figure 1.** Details of macrostructure and microstructure of titanium substrates from which the disk samples were cut.

Gram-positive Staphylococci biofilms account for approximately 75% of PJI, as biofilm increases 500-5000 times more resistance to antibiotics than planktonic cells [9–11]. Additionally, owing to its high adaptability and frequent exposure to antibiotic therapies, *Staphylococcus aureus* has undergone inadvertent selection for drug-resistant strains, leading to therapeutic failures [12–15]. The conventional treatments often require multiple surgeries and extended antibiotic therapy resulting in high morbidity and poor patient outcomes [7,16–21]. Novel techniques for preventing bacterial seeding onto orthopedic implants are of paramount interest.

Bioactive surface coatings have been studies extensively for the numerous benefits of imparting antibacterial and other properties to the selected substrates [22–27]. Layer-by-layer (LbL) self-assembly is a simple, easy, and versatile technique for building multilayers on a biomaterial by alternating coating applications of oppositely charged polyelectrolytes [28–30]. This process forms a polyelectrolyte multilayer (PEM), that improves osteoblast adhesion and proliferation and reduces bacterial colonization and growth [29]. Chitosan and alginate are well-studied, abundant, naturally derived, non-toxic and biocompatible polyelectrolytes with innate antimicrobial and osteoconductive properties [31,32]. The LbL assembly process is a very versatile technique and can be applied to almost any surface with a two or three-dimensional configuration.

Conversely, metal nanoparticles (mNPs) have attractive antimicrobial properties through metal ion release (bactericidal), oxidative stress, and non-oxidative mechanisms [33–38]. Silver nanoparticles (AgNPs) have long been considered for their antibacterial capacity, although their cytotoxicity has significantly hindered their progress towards clinical application [22,39–42]. In contrast, titanium dioxide nanoparticles ($TiO_2$NPs) have shown antibacterial efficacy while demonstrating better cytocompatibility [43–46] and even promoting the bone formation, owing their osteconductive properties [44,47–50]. The particle's surface area to volume of the prticle determines the binding and ion release properties that are crucial for antimicrobial activity. This relationship between size and reactivity (or antimicrobial activity) is inversely related. This potency is a metal ion release rate measure, where the higher relative surface area (and thus smaller size) allows for a greater ion release rate [22,33,34,51]. In the context of the medical application mentioned above, titanium would be the base material used as a substrate for these applications due to its ubiquitous presence in orthopedic surgery.

The aim of this work was to fabricate a $TiO_2$-based nanoparticle-imbedded PEM coating on highly porous titanium substrates using the LbL self-assembly technique. The hypothesis was that when mNPs are encapsulated in the PEM, the coating would provide an effective antibacterial property and would minimize the risk of antibiotic resistance while enhancing the osteogenic cell viability and proliferation on the coating. To verify this hypothesis, a thorough study was conducted to quantitatively assess the coating's antibacterial activity and osteoblastic cell proliferation. First, we

 doi:10.20944/preprints202310.0493.v1



developed and characterized PEM coating with imbedded $TiO_2$NPs and AgNPs (control) on porous titanium substrates. The In vitro viability and differentiation of MC3T3-E1 pre-osteoblast cells cultured on the coating as well as the antimicrobial activities of coated titanium substrates against *S. aureus* were assessed through a side-by-side comparison of $TiO_2$NPs and AgNPs. Our goal was to establish a proof-of-concept for the use of these methods and formulations to guide advance toward more effective infection prevention and enhanced bone growth of orthopedic implants.

## 2. Materials and Methods

### *2.1. Materials*

Titanium rods were purchased from Amplify Inc. (Scarborough, Maine, USA). High molecular weight chitosan (>90% deacetylated) was purchased from MP Biomedicals (Ohio, USA). Alginic acid sodium salt (alginate), silver nanopowder (<100 nm particle size, contains PVP as a dispersant), were purchased from Sigma Aldrich (Missouri, USA). $TiO_2$NP dispersion (rutile, 40-wt%, 30-50 nm) was purchased from Nanostructured and Amorphous Materials Inc. (Texas, USA). Alpha MEM media without phenol red ($\alpha$MEM), AlamarBlue and Fetal Bovine Serum (FBS) were purchased from Thermo Fisher Scientific (Massachusetts, USA). Alpha-MEM cell culture medium with nucleosides & without ascorbic acid ($\alpha$MEM+) was purchased from Invitrogen (Massachusetts, USA). MC3T3-E1 murine pre-osteoblast cells and MSSA (DNC274, ATCC 29213) were purchased from ATCC (Virginia, USA). Alkaline hosphatase Assay Kit (Colorimetric) was purchased from Abcam (Cambridge, UK). Luria-Bertani broth (LB Broth Miller) was purchased from BioShop (Ontario, Canada).

### *2.2. Bacterial strains*

The standard strains of *S. aureus* DNC274 and ATCC 29213 were cultured on LB media for 24 h. A single colony was picked and cultured in LB media supplemented with 2 % glycerol and stored at -80 °C until used for antimicrobial testing.

### *2.3. Titanium Substrate Preparation and Surface Functionalization*

The cylindrical semi-porous 3D-printed titanium rod of 4.5 mm in diameter and a length of 25 mm were used as substrate (Figure 1). Titanium rods were cut transversely to produce approximately 3 mm thick disks. Coronally, one half of the substrate was solid titanium, while the other half had a porous microstructure with a 400 µm average pore size, a 300 µm strut diameter, and was approximately 65% porous. Prior to LbL deposition, chemical crosslinking was adapted from Martin et al. [52] to achieve surface functionalization by amine groups. All cut semi-porous titanium disks were washed three times, 10 minutes at a time, in acetone, ethanol, and then ultrapure water, and then blown dry with inert nitrogen gas. Disks were carefully submerged in piranha solution and stirred for 1 h to further clean and hydroxylate specimens. Disks were then removed from the solution and washed three times in ultrapure water. To produce amino-functionalized disks, samples were immersed in a 2% solution of (3-aminopropyl) triethoxysilane (APTES, Sigma Aldrich, Missouri, USA) for 1 h. Samples were then washed five times with acetone to remove any residual silane groups. To facilitate and enable the deposition and crosslinking of the primary polymer layer, samples were then treated in 4% glutaraldehyde solution under stirring for 8 h. Samples were then removed and washed thrice in ultrapure water. The primary chitosan layer was applied by immersing samples in 0.1% chitosan solution for 8 h, and then rinsing non-adhered chitosan from the surface with ultrapure water.

### *2.4. $TiO_2$ and Ag Nanoparticles Size Measurement*

Prior to the experiments, the AgNPs and $TiO_2$NPs were suspended in water and their size distribution was examined for using the Nanosight NS300 Nanoparticle Tracking Analyzer (NTA, Salisbury, UK) to ensure that the purchased materials met the specifications on their labels. 1 mg/mL

 doi:10.20944/preprints202310.0493.v1



suspensions were prepared using water as the diluent and then diluted 500-fold to allow effective and accurate size measurements.

*2.5. Preparation of mNP Suspension Prior to Encapsulation in LbL Coating*

To prepare three different concentrations of alginate-$TiO_2$NPs suspensions, 40 wt% aqueous stock suspension of $TiO_2$NPs (calculated to an equivalent of ≈ 670 mg/mL), was first diluted using ultrapure water to a concentration twice that of the final desired concentration of the most concentrated dispersion group. An aliquot of this initial stock suspension was diluted to a concentration of ≈ 55 mg/mL by adding 1.2 mL of stock suspension to ≈ 14 mL of ultrapure water. 7 mL of 0.2% alginate, 1.75, 3.5 or 7 mL of the diluted $TiO_2$NPs were transferred into three 15 mL tubes, mixed, and then filled with ultrapure water to a final volume of 14 mL, to achieve a final alginate concentration of 0.1% and $TiO_2$NP concentrations of ≈ 7±1, ≈ 14±1, and ≈ 28±1 mg/mL. Suspensions were vortexed vigorously for 1 minute each to achieve uniform dispersions.

To prepare two different concentrations of alginate-AgNPs suspensions, PVP-coated nanosilver powder was dispersed in ultrapure water at a concentration twice that of the highest intended AgNPs group concentration. Stock dispersions were made to a concentration of 8 mg/mL. To ensure unifrom dispersion, the solution was vortexed vigorously for 1 minute, and then bath-ultrasonicated for 1 h. Meanwhile, 7 mL of 0.2% alginate was added to 2 separate 15 mL tubes. When ready, AgNP suspensions were added to the tubes containing alginate solutions, and filled to a final volume of 14 mL with ultrapure water, to obtain final alginate concentrations of 0.1% and AgNP concentrations of 0.4, and 4 mg/mL.

*2.6. Preparation of the Polyelectrolytes for LbL Deposition*

0.2% chitosan solution was prepared by adding 20 mg/mL (0.2 g/100mL) chitosan powder to 1% glacial acetic acid and stirring overnight until completely dissolved. Immediately prior to all experiments, aliquots of appropriate volume were isolated, and the pH was adjusted to 6.0 using 10 M and 1 M sodium hydroxide. The final concentration of the chitosan solution was then adjusted to 0.1% with ultrapure water.

0.2% alginate solution was prepared by adding 20 mg/mL (0.2 g/100mL) sodium alginate powder into double-distilled water and stirred overnight. For experimental conditions using alginate without nanoparticles, aliquots were further diluted to a concentration of 0.1%.

*2.7. mNP imbedding and LbL Coating Procedures*

After the surface functionalization of the titanium substrate (section 2.3), the subsequent coating of the multilayers was performed according to the protocol adapted from Zhong et al. [30]. Briefly, each polymer layer was applied similarly to the above layers, where the samples were immersed in 15 mL centrifuge tubes containing chitosan/alginate and rotated for 15 minutes to obtain a homogenous coating. After removal, the samples were washed twice in ultrapure water to remove unadsorbed polymer from the sample surface. Samples were then immersed in the appropriate subsequent solution/suspension. This process was repeated until the desired number of bilayers were applied, at which point the disks were washed and air-dried overnight.

Samples coated with alginate containing ≈ 7±1, ≈ 14±1, and ≈ 28±1 mg/mL of $TiO_2$NPs were labelled 10 $LbL^+[TiO_2NP]_l$, 10 $LbL^+[TiO_2NP]_m$, and 10 $LbL^+[TiO_2NP]_h$, respectively. Samples coated with alginate containing 0.4 and 4 mg/mL of AgNPs were labelled 10 $LbL^+[AgNP]_l$ and 10 $LbL^+[AgNP]_h$ respectively. Samples coated using alginate without nanoparticle additives were labelled as 10 $LbL^-$NP, representing a PEM made of otherwise unmodified chitosan and alginate. Control samples, *i.e.*, uncoated Ti substrate (or bare) were labelled as B (Table 1).

Preprints (www.preprints.org) | NOT PEER-REVIEWED | Posted: 9 October 2023 doi:10.20944/preprints202310.0493.v1



**Table 1.** Samples' descriptions and abbreviations.

| Sample description | Experiments | Abbreviation |
|---|---|---|
| • Uncoated Ti substrate (bare) | • AFM/QCM-D | **B** |
| • With 2 bilayer of Chitosan/Alginate no nanoparticles (NP) | • AFM/ QCM-D | **4 LbL⁻NP** |
| • With 4 bilayer of Chitosan/Alginate no NP | • AFM/ QCM-D | **8 LbL⁻NP** |
| • With 4 bilayer of Chitosan/Alginate with 28 mg/mL $TiO_2$ NP | • AFM/ QCM-D | **8 $LbL^+[TiO2NP]_L$** |
| • With 5 bilayer of Chitosan/Alginate no NP | • Viability/ALP/Antimicrobial assay | **10 LbL⁻NP** |
| • With 5 bilayer of Chitosan/Alginate with 7 mg/mL $TiO_2$NP [low] | • Viability/ALP/Antimicrobial assay | **10 $LbL^+[TiO_2NP]_l$** |
| • With 5 bilayer of Chitosan/Alginate with 14 mg/mL $TiO_2$NP [medium] | • Viability/ALP/Antimicrobial assay | **10 $LbL^+[TiO_2NP]_m$** |
| • With 5 bilayer Chitosan/Alginate with 28 mg/mL $TiO_2$NP [high] | • Viability/ALP/Antimicrobial assay | **10 $LbL^+[TiO_2NP]_h$** |
| • With 5 bilayer Chitosan/Alginate with 0.4 mg/mL AgNP | • Viability/ALP/Antimicrobial assay | **10 $LbL^+[AgNP]_l$** |
| • With 5 bilayer Chitosan/Alginate with 4 mg/mL AgNP | • Viability/ALP/Antimicrobial assay | **10 $LbL^+[AgNP]_h$** |

*2.8. Investigation of LbL Deposition Using Quartz Crystal Microgravimetry with Dissipation (QCM-D)*

The in situ LbL build-up was determined by a QSense QCM-D Analyzer (Biolin Scientific Inc., Gothenburg, Sweden) instrument. To best mimic the surface properties of the semi-porous titanium implant samples that were used in all other experiments, QCM-D titanium crystals (QSX 310) (Biolin Scientific Inc., Gothenburg, Sweden) were employed as substarte. However, in the chitosan and alginate LbL build-up, the polyelectrolyte solutions were run through the system on the bare Ti-based crystals without a prior surface functionalization, as the acid treatment could damage the Ti crystals.

Ti crystals were cleaned by UV-Ozone (UV–ozone chamber Bioforce Nanosciences, Inc., Virginia, United States) treatment for 10 minutes, washed 5 minutes in a 5:1:1 mixture of ultrapure water, 25% ammonia, and 30% hydrogen peroxide at 75 $^0$C, followed by 10 minutes UV-Ozone treatment. The experiment was set up to oscillate the crystals at their fundamental resonance frequency ($f$ = 4.95 MHz), and their odd overtones (3-11) using electrodes supplying a radiofrequency voltage. The LbL process began with water flowing into the chambers at a rate of 400 µL/minute for 5 minutes to establish a baseline measurement. Chitosan was then flowed in at the same rate for 3 minutes to ensure that the entire crystal was covered with the polymer. At this point, the flow pump was stopped for 15 minutes, to allow the polymer to adsorb onto the crystal surface. Water was then pumped for 3 minutes to remove unadsorbed polymer. The tubing was switched to the alginate solution, and the same process was followed. The procedure was repeated until a total of five bilayers was applied. Frequency and dissipation measurements were performed in real time using QSoft QCM-D software, while viscoelasticity and thickness calculations were performed using the Voigt-based viscoelastic model in the QTools software.

*2.9. Analysis of Surface Morphology and Roughness of coated Substrates by Microscopy Techniques*

The FEI Quanta450 Environmental Scanning Electron Microscope (ESEM) was used to further confirm the deposition of the PEM, as well as to examine its porous microstructure before cell culture. The SEM was set to a full vacuum, and samples were lifted on the platform to a distance of 10 mm from the camera. Samples from each group were imaged at 5-10 kV, final images were taken over 10 seconds for increased resolution.

Samples following MC3T3-E1 cell culture assays were also imaged with SEM for visualization of cell adhesion and spreading on the substrate surface. To prepare samples for this set of images, culture media was removed from the wells, and samples were washed thrice with phosphate buffered saline (PBS), before fixation using 4% paraformaldehyde for 1 h. Samples were then rinced

with PBS and processed for dehydration, by immersion in graded concentrations of ethanol from 30%, 50%, 70%, 80%, 90% to 100% for 15 minutes each. Subsequently, samples were dried by critical point drying, and coated using a platinum sputter coater.

A MultiMode 8-HR AFM (Bruker, Massachusetts, USA) was used to evaluate the surface roughness and morphology for non-functionalized bare titanium disks, disks coated with two bilayers or four bilayers, with $TiO_2$NPs and without $TiO_2$NPs. All samples were prepared following the same procedure as those for cell culture and other experiments. PeakForce mode in air was used for all images, using a silicone probe with a spring constant k = 0.35 N/m, and a resonance frequency $f_0$ = 65 kHz. Images were acquied in 20 × 20 μm sections.

*2.10. Cytotoxicity Assay*

MC3T3-E1 cells ($1 \times 10^6$) were cultured in 10 mL of αMEM+ supplemented with 10% FBS and 1% penicillin/streptomycin in a T-75 flask. Every 2-3 days, the cell culture media refreshed until approximately cells reached 80% confluence, at which time adherent cells were collected from the surface of the flask was performed by removing the culture medium, gently washing with PBS, and then incubating for 5 minutes in 2 mL of 0.25% trypsin/EDTA. 5 mL of αMEM+ was added to the flask to resuspend the detached cells. The cells were inactivated with trypsin and were transferred to a 15 mL centrifuge tube. The cell density of the suspension was calculated using an automated cell counter to determine the volumes required for experimental seeding densities. Cells were centrifuged to attain pellet and were resuspended with fresh αMEM-. The titanium disks were sterilized according to Holmes et al. [53]. Briefly, samples were immersed in 70% ethanol for 1 h, and further washed in an serial ethanol dilution of 35%, 17.5%, 8.75% for 30 minutes. The disks were then washed three times for 10 minutes at a time in sterile 1 × PBS (pH 7.4) to remove any residual ethanol. After sterilization, specimens were placed in triplicate into wells of a 48-well microtiter plate. The wells without titanium disks placed inside were used as positive growth controls. 400 μL MC3T3-E1 cells ($3 \times 10^4$ cells/mL) were then seeded and incubated for the predefined time points in a $CO_2$-controlled incubator at 37 $^0$C. αMEM- medium was refreshed every 3 days and 24 hours prior to collection/testing time points for cell viability and differentiation assays.

The percent Difference was used as a measure of relative cell viability of the experimental groups compared to control wells seeded with preosteoblasts without sample exposure. The calculation provided a quantitative description of how much more/less cell growth occured in our experimental groups, compared to how much cell growth was observed in positive control wells in order to determine the relative efficacy of the treatment.

*2.11. MC3T3-E1 Viability Assessment by AlamarBlue*

On days 1 (24 h after initial seeding), 4, 7, and 14, the cells were stored at -80 $^0$C for later assessment of ALP activity. Fresh 400 μL of αMEM- media containing 10% AlamarBlue (9:1 ratio between cell culture medium and AlamarBlue) was added to the wells and incubated for 4 hours in the dark. After incubation, 100 μL from each well was withdrawn in triplicate, and added to 96-well clear flat-bottom UV-transparent microplate (Sigma Aldrich, Missouri, United States). The wells of the 48-well plate were once again replenished with 400 μL of αMEM-, and returned to the incubator. A Spectramax i3 spectrophotometer (Molecular Devices, California, United States) was used to measure the absorbance values of the media samples at 570 nm and 600 nm. The percentage difference in AlamarBlue reduction was calculated from the absorbance data and the extinction coefficients of resazurin according to the protocol provided by the manufacturer.

*2.12. Assessment of MC3T3-E1 osteogenic differentiation by ALP Activity Analysis*

On days 1, 4, 7, and 14 of cell culture with coated disks, αMEM- cell culture medium was extracted from each well, and alkaline phosphatase (ALP) activity assays were performed on the above-mentioned media extracts according to the ab83369 Alkaline Phosphatase Assay Kit (Colorimetric) manual. Briefly, a standard curve was generated prior to assaying the experimental

 doi:10.20944/preprints202310.0493.v1



samples. 80 µL of each sample was poured into each well of a 96-well microtiter plate, 80 µL of media control group, and 120 µL of each standard dilution. Further, 20 µL of Stop Solution was added to the control wells, along with 50 µL of 5 mM para-nitrophenyl phosphate (pNPP) to the sample and control wells. 10 µL of ALP enzyme was added to each of the standard dilution wells. Plates were covered with foil to protect from light and incubated at 25 °C for 60 minutes, followed by the addition of 20 µL of Stop Solution to the sample and standard wells. The plates were gently vortexed, and colorimetric measurements were performed usinga Spectramax i3 spectrophotometer (Molecular Devices, California, United States) at 405 nm.

### *2.13. Antimicrobial Assessment of Coated Ti substrates*

*S. aureus* (DNC274, ATCC 29213) strains were grwn on LB agar plates from the glycerol stocks. A single colony was transferred to 5 mL LB media and incubated at 37 $^0$C for 6 hours and further subcultured into 15 mL LB media with $OD_{600}$ 0.05, and then incubated overnight at 37 $^0$C at 200 rpm. The next day, the cultures were centrifuged to remove the media, and the pellet was washed twice with 1 × PBS and resuspended in LB media. The OD was adjusted to 0.05 OD (~1 × $10^4$ CFU/mL). The coated titanium disks along with the appropriate controls were placed in a 48-well microtiter plate, seeded with 400 µl of *S. aureus* suspensions at 1 × $10^4$ CFU/mL, and incubated at 37 °C for 24 hours without shaking. After 24 hours of incubation, the planktonic bacterial growth was determined by removing 100 µL of suspension from each sample well and transferred it in triplicate to a 96-well microtiter plate. These samples were serially diluted 10-fold and plated onto LB agar and incubated overnight at 37 °C, and the CFUs were determined by colony counting. The cells in the 48 well microtitre plates were removed and gently washed thrice with 1 × PBS, and titanium discs were transferred to 1.5 mL Eppendorf tubes containing 1 mL of 1 × PBS. These tubes were then vortexed at high intensity for 1 minute to detach adhered bacteria and resuspend them into 1 × PBS. These samples were further serially diluted and plated, and colony counts were determined as CFU.

### *2.14. Statistical Analysis*

Statistical comparison between samples was performed by two-way analysis of variance (ANOVA) Tukey's post-hoc comparisons was performed by Prism5. Values are means from at least 3 parallels. Bars are standard deviations (SD). Differences were considered statistically highly significant at $p < 0.01$.

## 3. Results and discussion

### *3.1. Nanoparticle Characterization*

The average size of theAgNPs was 77.9 nm; and 50 % were below 100 nm as determined by NTA (Figure 2A). Although the mean was higher than intended, likely due to some aggregation producing larger particles, the distribution of particle sizes was effectively unimodal at about 45.6 nm. These results support the method used to suspend the purchased AgNPs. The distribution of $TiO_2$NPs sizes (Figure 2B) from the purchased nanoparticle suspension had a narrow unimodal peak at 39.2 nm, and an average diameter of 39.4 nm. which is consistent with the manufacturer of rutile $TiO_2$NPs.

Preprints (www.preprints.org) | NOT PEER-REVIEWED | Posted: 9 October 2023 doi:10.20944/preprints202310.0493.v1



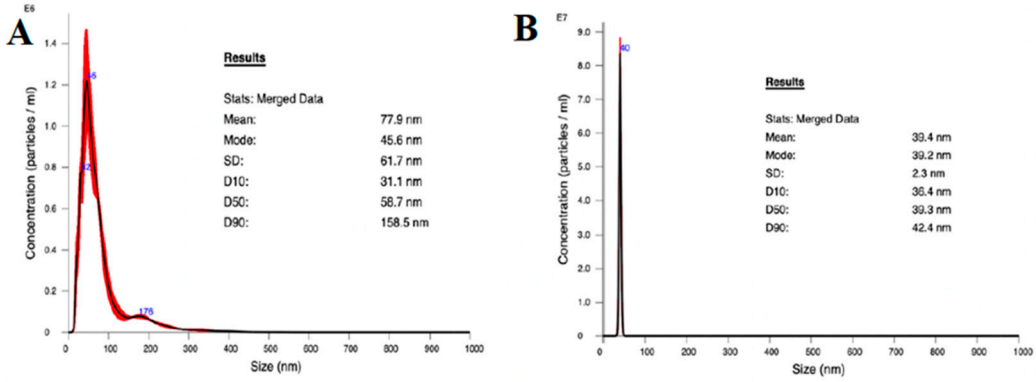


**Figure 2.** Nanoparticle size distribution as measured by NTA. A) $TiO_2$NP and B) AgNP.

*3.2. Validation of LbL Deposition Using QCM-D and PEM Coating Characterization*

To validate the LbL self-assembly of the PEM, its simulated in situ build-up was achieved using QCM-D. The frequency decreased linearly along the LbL process, indicating the consistent sequential build-up of the PEM on the titanium dioxide quartz crystal (Figure 3A). Dissipation measurements followed the frequency changes (Figure 3B), while viscoelasticity and thickness increased stepwise with each bilayer (Figure 3C and D respectively). From the thickness plot (Figure 3D) at the first and last water flow stages, the thinnest layer had a thickness of $5.4982 \times 10^{-14}$ m (≈ 0.05 picometer) and reached to a thickness of $1.8529 \times 10^{-8}$ m (≈18.5 nm) after deposition of 8 layers of polyelectrolytes. This final PEM was thinner than anticipated, possibly due to the flow rate. A study indicated an increase in the thickness of PME when the water flowed at 100 µL/minutes, compared to 400 µL/minutes [21]. The frequency change immediately after the washing step, also showed a sharp increase, which could be associated with the some loss of polymer electrolytes, potentially destabilizing the subsequent polymer depositions, further explaining the formation of a thinner coating in-situ. A thicker PME deposition can be expected for the functionalized titanium substrates used for all other experiments, as the absence of surface functionalization could have contributed to reduced adsorption of the initial layer.

Examples of the electron microscopy micrographs of coated titanium substrates are shown in Figure 3E-F. Using a dotted line as a visual aid, the top-down view of the sample in Figure 3E denotes the structural distinction between the solid and porous sides of the substrate. These images demonstrate the successful coating of the titanium substrates with the PEM. The porous structure created by the PEM has been reported to promote bone ingrowth [55,56].

The QCM-D results for PEM were confirmed by AFM analysis. The AFM images showed that the application of PEM smoothed the surface of the substrates, as a decrease in surface roughness was observed by the deposition of PEM onto the titanium substrates compared to bare group (Figure 3 right panels and Figure 3G). This was particularly evident when considering the relative smoothing of the surface upon multilayer adsorption, where the comparatively high average roughness in the bare sample (Ra = 91.3 nm) is no longer reflected in samples with even only 4 LbL (Ra = 11.2 nm). The subsequent increase in Ra after additional PEM deposition, i. e., 8 LbL (17.0 nm), although no significant, could be attributable to an increase in the porosity of the multilayer film [55]. As expected, the surface roughness increased when the $TiO_2$NPs was embedded in the PEM coating (17.0 nm for 8 $LbL^-$NPs versus 71.2 nm for 8 $LbL^+[TiO_2NPs]_h$. The results indicated that the nanoparticles were within the appropriate size range and sufficiently monodispersed to evenly cover the entire substrate (including within the porous titanium lattice) with the PEM. Although this was a rare occurrence, the large peak on the AFM image of 8 $LbL^+[TiO_2NPs]_h$ denoted with an arrow, indicated that titanium nanoparticle might undergo aggregation. Overall, this increase in surface roughness after the encapsulation on the NPs is a beneficial characteristic, as it has been shown that cell adhesion and bone-implant contact are improved with higher roughness [57].

Preprints (www.preprints.org) | NOT PEER-REVIEWED | Posted: 9 October 2023 doi:10.20944/preprints202310.0493.v1



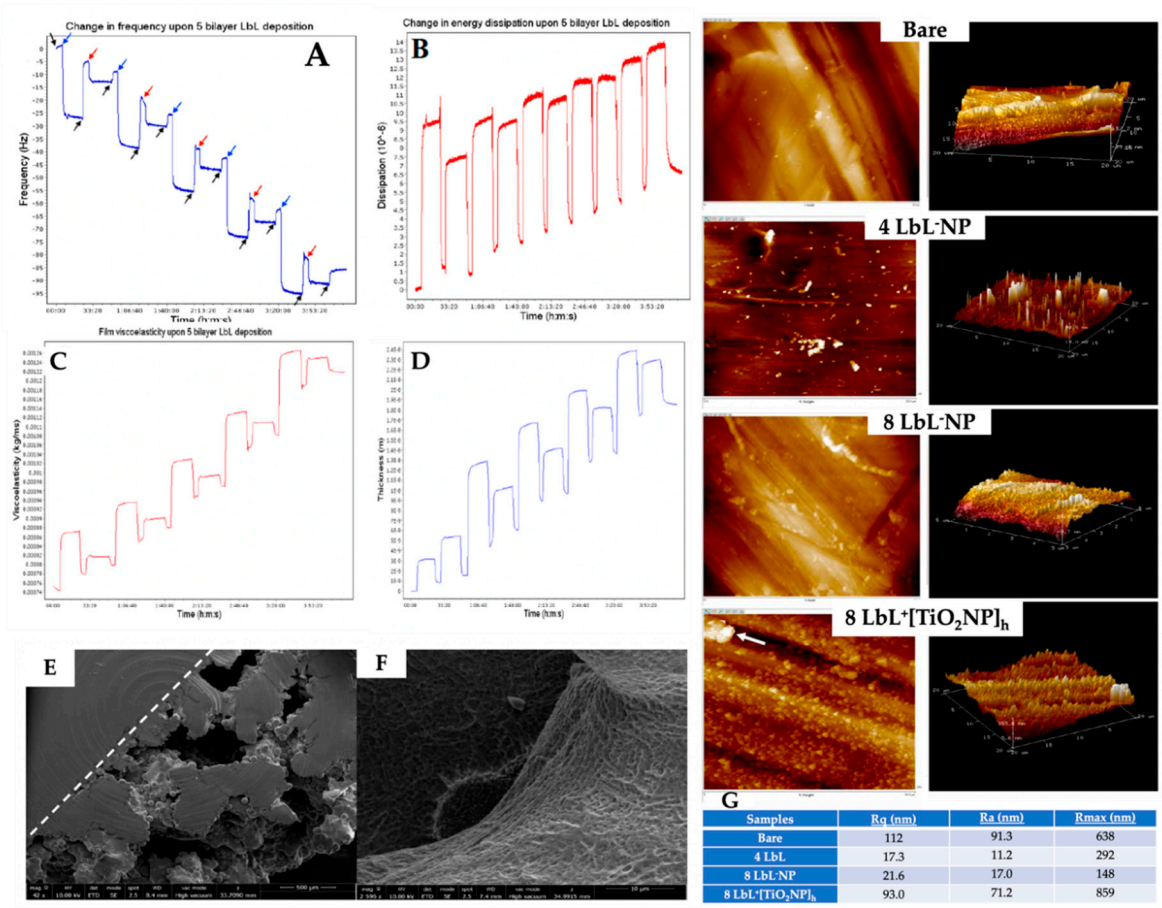


| Samples | Rq (nm) | Ra (nm) | Rmax (nm) |
|---|---|---|---|
| Bare | 112 | 91.3 | 638 |
| 4 LbL | 17.3 | 11.2 | 292 |
| 8 LbL-NP | 21.6 | 17.0 | 148 |
| 8 LbL+[TiO2NP]h | 93.0 | 71.2 | 859 |

**Figure 3.** Panels A-D: QCM-D plot of A) the change in frequency (Hz) over tone of a titanium oxide-coated quartz crystal undergoing LbL application of 5 bilayers of chitosan and alginate polyelectrolytes. Arrows denote time points at which specific solutions were applied. Black - ultrapure water, Blue - chitosan, Red – alginate; B) Change in dissipation; C) Changes in viscoelastic properties; and D) Change in film thickness over the coating period. Panels E-F: SEM images of E) Top-down view of semi-porous titanium showing the structure's solid and porous sides of the PEM-coated titanium and F) Close-up view into a pore of a sample coated with chitosan and alginate shows successful PEM application and penetration into the pore. The two panels in the right show typical 2-D and 3-D AFM images of bare titanium substrate, with 4 LbL-NP, 8 LbL-NP; $^{+}[TiO_2NPs]_h$ (≈ 28 mg/mL $TiO_2$NPs: Arrow denotes a potential agglomeration of $TiO_2$NPs) and G) Surface roughness for different titanium substrates as determined by AFM. Scale bars vary with the images.

### *3.3. MC3T3-E1 Viability and Proliferation on PEM Coated Ti Substrates*

Viabilityof pre-osteoblast MC3T3-E1 cells on LbL$^{+}$ $TiO_2$NP was determined at 1, 4, 7 - days time points by AlamarBlue using LbL-NP as negative control and uncoated samples along with those LbL coated imbedding AgNPs as positive controls (Figure 4A). This analysis showed a significant difference in cell viability among various time points (n=3) (n=3; $p < 0.0001$) and groups (n=3; $p < 0.0001$) as well as between the two variants when combined (n=3; $p < 0.0001$). Coating significantly affected the viability of MC3T3-E1 cells at a given time and across days. Data were also categorized by the day of testing, as shown in Figure 4A. After day 1, samples 10 LbL$^{+}[TiO_2NP]_m$ showed higher cell viability than all other test groups (n=3; p $< 0.0003$), while the others performed similarly. On day 4, these same cells maitained their superior viability (n= 3; $p < 0.05$) compared to to all other groups. As expected, cells exposed to 10 LbL$^{+}[AgNP]_h$ experienced a reduction in relative viability, resulting in these showing less viability than all other groups (n=3; $p < 0.0001$). At day 7, regardless the titanium oxide NP concertation used, there was no significant difference among these samples and the most significant remaining difference between the groups was the sustained reduction in viability in 10 LbL$^{+}[AgNP]_h$, which was still lower than all other groups (n=3; $p < 0.0001$). This is a

Preprints (www.preprints.org) | NOT PEER-REVIEWED | Posted: 9 October 2023 doi:10.20944/preprints202310.0493.v1



very interesting finding considering that much higher concentration of titanium oxide NPs was used compared to AgNPs for cell viability, confirming much lower cytotoxicity of titanium NPs to osteoblastic cells.

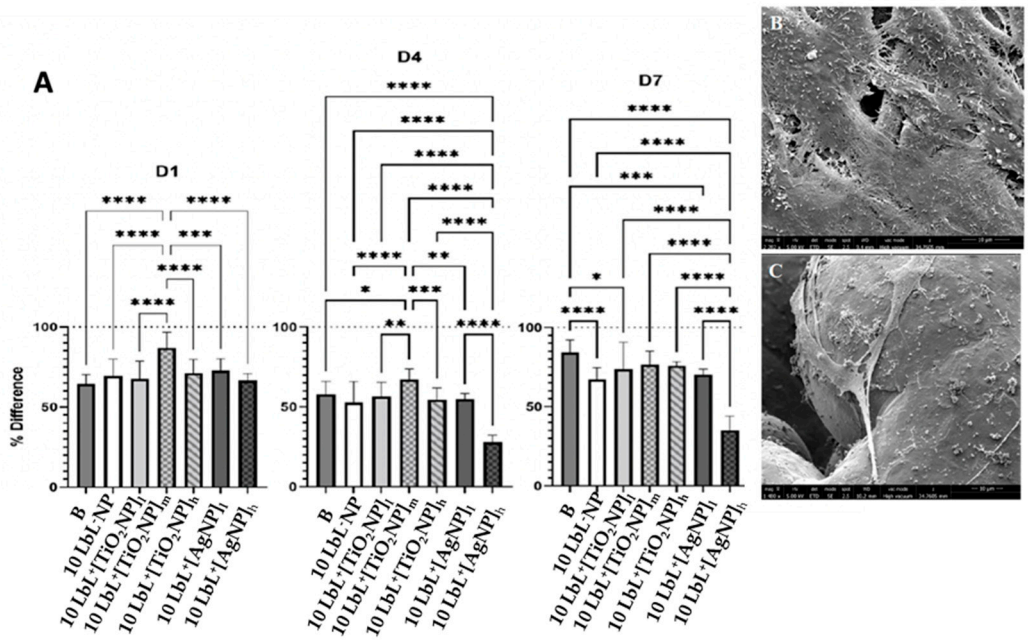


**Figure 4.** Panel A are the plots of AlamarBlue tests of percent difference across test days. D1 - after 1 day, D4 - after 4 days; D7 - after 7 days. Dotted line at y = 100 refers to the measured AlamarBlue results of the reference group (cells only, no samples). Stars denote significant differences(n=3), * - < 0.05; ** - < 0.01; *** - < 0.001; **** - < 0.0001. Group labels are defined as 10 $LbL^{-}NP$ – with 5 bilayers of Chitosan/Alginate without NP, 10 $LbL^{+}[TiO_2NP]_l$ - with 5 bilayers of Chitosan/Alginate with 7 mg/mL TiO2NP, 10 $LbL^{+}[TiO_2NP]_m$ - with 5 bilayers of Chitosan/Alginate with 14 mg/mL TiO2NP, 10 $LbL^{+}[TiO_2NP]_h$ - with 5 bilayers of Chitosan/Alginate with 28 mg/mL, 10 $LbL^{+}[AgNP]_l$ - with 5 bilayers of Chitosan/Alginate with 0.4 mg/mL AgNP; 10 $LbL^{+}[AgNP]_h$ - with 5 bilayers of Chitosan/Alginate with 4 mg/mL AgNP, B – uncoated Ti Substrate (Bare). B) and C) SEM images of titanium substrate surfaces showing MC3T3-E1 adhesion and spreading on 10 $LbL^{+}[AgNP]_h$ on the solid and porous parts of the substrate (scale bar: 10 µm).

To determine whether the presence of NPs affects the MC3T3-E1 cells osteogenic differentiation, the ALP activity was conducted on extracted cell culture media to determine the extent of preosteoblast differentiation using alkaline phosphatase as a biomarker (Figure 5A). In these assays, groups were also separated based on the polymer layer applied as the uppermost coating; nanoparticle-incorporated alginate or chitosan. The results were consistent with the previous literature [58,59]. Despite a significant effect of the top-coat on day 7 (n=3; $p = 0.0001$), this difference was not seen on any other day tested, indicating that the top coat was not a significant factor in the ALP activity of cells exposed to samples throughout the experimental period. Therefore, MC3T3-E1 analyses were conducted with those groups combined. A two-way ANOVA was performed on the combined ALP data, and it was found that there was a main effect of day (n=3; $p < 0.0001$), of group (n=3; $p < 0.0001$), and an interaction of group × day (n=3; $p < 0.0001$). There were no statistical differences between the groups on days 1 and 4. On day 7, cells exposed to samples 10 $LbL^{+}[TiO_2NP]_h$ samples showed slightly higher ALP activity compared to those exposed to 10 $LbL^{+}[TiO_2NP]_l$ (n=3; $p = 0.0453$). Tests on day 14 showed a significant increase in ALP activity in all groups compared to their respective counterparts on previous days. Within day 14, cells exposed to 10 $LbL^{+}[AgNP]_l$ showed one of the highest absolute means of ALP activity (0.01528 µmol/minute/mL), second only to the cell-only control group (0.01530 µmol/minute/mL). This increased ALP activity was greater than that of the

Preprints (www.preprints.org) | NOT PEER-REVIEWED | Posted: 9 October 2023 doi:10.20944/preprints202310.0493.v1



groups without nanoparticles (n=3; $p < 0.05$), with 10 LbL$^+$[TiO$_2$NP]$_m$, 10 LbL$^+$[TiO$_2$NP]$_h$ (n=3; $p < 0.001$), but not statistically different from those exposed to 10 LbL$^+$[TiO$_2$NP]$_l$ and 10 LbL$^+$[AgNP]$_h$.

A linear regression was performed on an isolated data segment, focusing on the potential nanoparticle dose-dependent responses that cells may have to the construct. These data are presented in Figure 5B-C. Here, a difference in cell responses was observed depending on the nanoparticle concentration incorporated into the PEM. For TiO2NP-containing samples, a significant positive relationship between nanoparticle concentration and ALP activity was found in the chitosan-topped group ($R^2 = 0.0832$, $F(1,7) = 35.74$, n=3; $p = 0.0006$) but not the alginate-topped group. In AgNP-containing samples, a negative relationship was observed between concentration and ALP activity ($R^2 = 0.7328$, $F(1,4) = 10.97$, $p = 0.0296$) in the alginate group. This suggests that PEMs with higher concentrations of TiO2NPs, especially when coated with chitosan, may promote greater ALP activity, while alginate-coated PEMs with increasing concentrations of AgNPs show decreasing ALP activity in response.

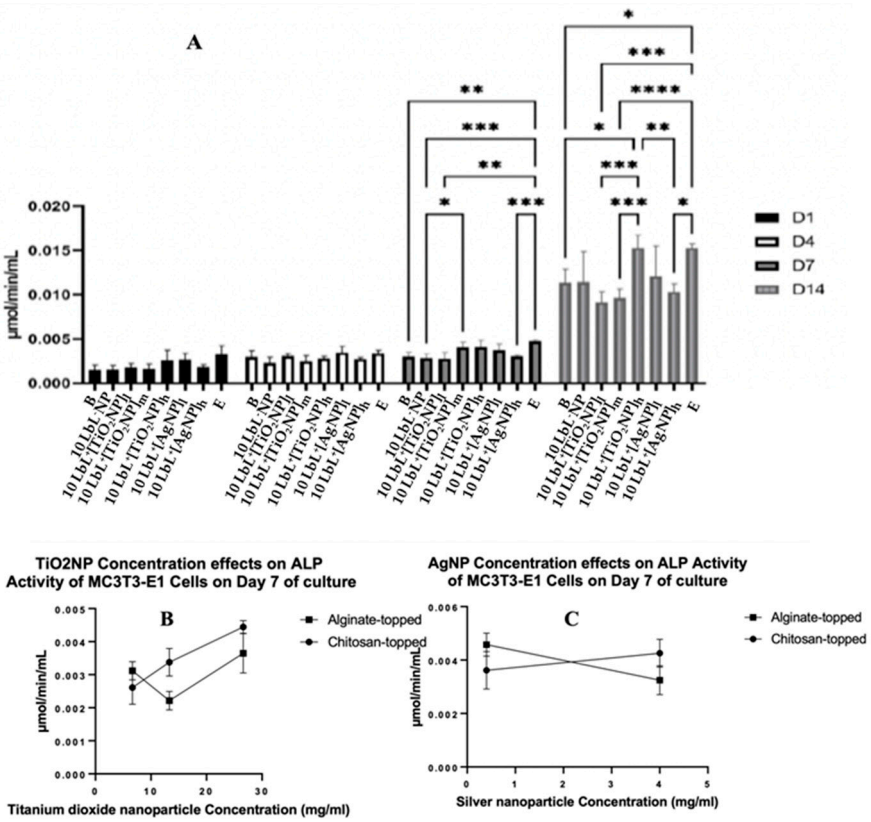


**Figure 5.** A) ALP activity of coated samples across test days where different top-coated groups are combined. Stars denote significant differences (n=3) * - < 0.05, ** - < 0.01, *** - < 0.001, **** - < 0.0001. Group labels are defined as 10 LbL-NP - with 5 bilayers of Chitosan/Alginate without NP, 10 LbL$^+$[TiO$_2$NP]$_l$ -with 5 bilayers of Chitosan/Alginate with 7 mg/mL TiO$_2$NP, 10 LbL$^+$[TiO$_2$NP]$_m$ - with 5 bilayers of Chitosan/Alginate with 14 mg/mL TiO$_2$NP, 10 LbL$^+$[TiO$_2$NP]$_h$ - with 5 bilayers of Chitosan/Alginate with 28 mg/mL, 10 LbL$^+$[AgNP]$_l$ - with 5 bilayers of Chitosan/Alginate with 0.4 mg/mL AgNP, 10 LbL$^+$[AgNP]$_h$ - with 5 bilayers of Chitosan/Alginate with 4mg/mL AgNP, B – uncoated Ti Substrate (Bare) and E – cells only. Panels B-C: Linear regression plots of nanoparticle concentration on ALP activity of MC3T7-E1 cells exposed to nanoparticle-imbedded PEMs.

### *3.4. Antimicrobial activity*

The antimicrobial efficacy of the coated samples was tested on mature 24 h biofilm of *S. aureus* and CFU were determined. Bonferroni's multiple comparisons showed a distinct difference in the 10 LbL$^+$[TiO$_2$NP]$_h$ topmost polymer layer (n=3; $p = 0.0007$), and chitosan-topped 10 LbL$^+$[TiO$_2$NP]$_m$ and 10 LbL$^+$[TiO$_2$NP]$_h$ (n=3; $p = 0.0041$) (Figure 6A).

Preprints (www.preprints.org) | NOT PEER-REVIEWED | Posted: 9 October 2023 doi:10.20944/preprints202310.0493.v1



No significant statistical differences between nanoparticle types were observed. In the interest of understanding the potential dose-response characteristics of the antibacterial activity, nanoparticle-containing groups were isolated into their respective data sets, and a simple linear regression was performed on each of them (Figure 6A). For samples containing $TiO_2$NPs, a significant negative relationship was found between nanoparticle concentration and CFU in the alginate-topped group ($R^2 = 0.6798$, $F(1,7) = 14.86$, n=3; $p = 0.0063$) but no significance in chitosan-topped group. Surface charge affects protein absorption, cell adhesion, and proliferation. Positive charges can promote cell spreading, proliferation, and immune system signaling, leading to regenerative responses and better biocompatibility [60]. Surface charge density along with two primary forces, *i. e.*, van der Waals and electrostatic interactions also impact bacterial adhesion. Bacteria typically carry a net negative charge, resulting in greater adhesion to positively charged surfaces [61], however, the bacterial adhesion species specific *S. aureus* demonstrating higher adhesion on the cationic surfaces [62]. In AgNP-containing samples, a positive relationship was observed between concentration and bacterial growth ($R^2 = 0.7667$, $F(1,4) = 13.14$, $p = 0.0222$) in the alginate group. These data suggest a trend toward dose-dependent antibacterial activity in alginate-topped $TiO_2$NP-incorporated PEMs, although the magnitude of growth inhibition was less than anticipated. One source of this issue could be that the size of the wells in 48-well culture plate in which the samples were cultured with the suspended bacteria, was larger than the sample size. This could limit the bacteria exposure to the coating, and they could grow in liquid culture without direct contact with the coating. This could have given the bacteria the opportunity to multiply to a number that would be unmanageable by the coating. Another reason for observing such a result could be related to the seeding density and the culture materials used. Other studies have been conducted using widely varying methods and seeding densities (from $10^5$ CFU/mL [63] to $10^6$ CFU/mL [64], to $10^9$ CFU/mL [65]).

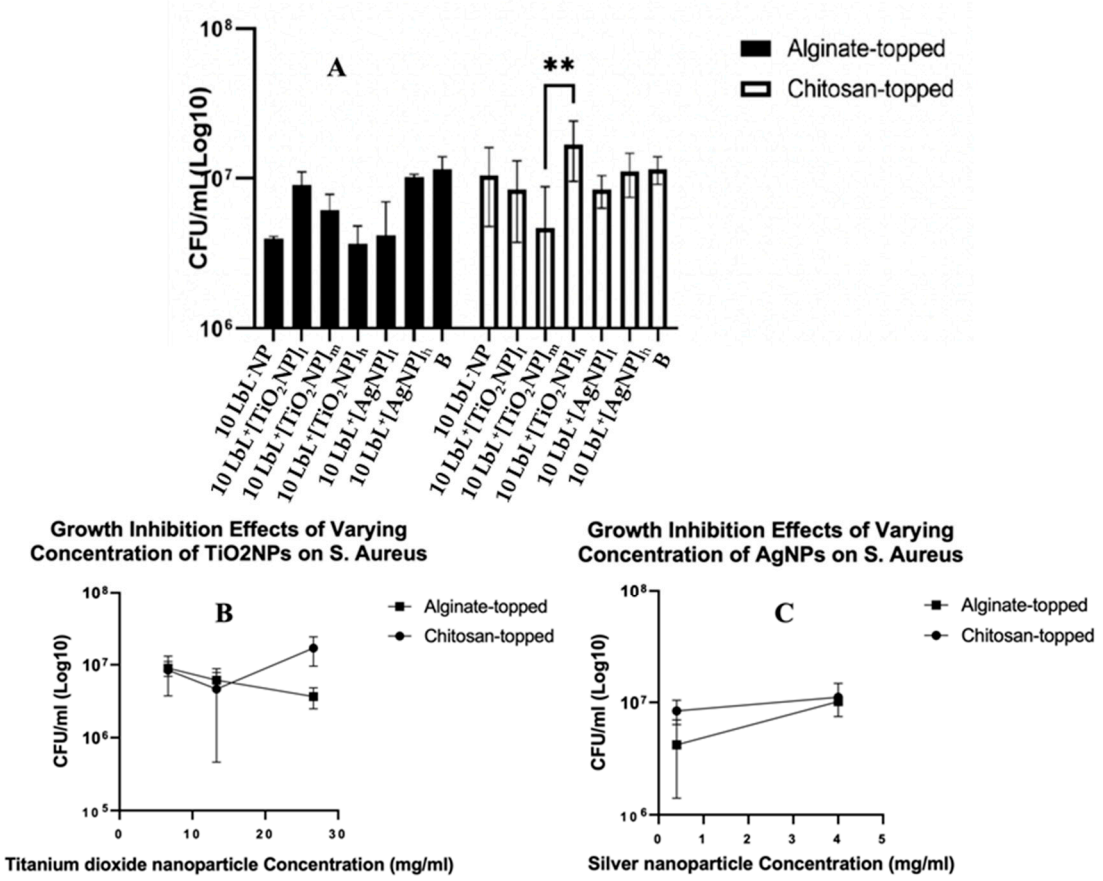


**Figure 6.** Panel A: Estimated bacterial growth based on cell counts of adherent bacteria exposed to samples in liquid media for 24 h. Stars denote significant differences (n=3), ** - < 0.01. Group labels are defined as 10 $LbL^-NP$ – with 5 bilayers of Chitosan/Alginate without NP; 10 $LbL^+[TiO_2NP]_l$ – with 5 bilayers of Chitosan/Alginate with 7 mg/mL $TiO_2$NP; 10 $LbL^+[TiO_2NP]_m$ -with 5 bilayers of

Chitosan/Alginate with 14 mg/mL $TiO_2$NP, 10 $LbL^+[TiO_2NP]_h$ - with 5 bilayers of Chitosan/Alginate with 28 mg/mL; 10 $LbL^+[AgNP]_l$ -with 5 bilayers of Chitosan/Alginate with 0.4 mg/mL AgN, 10 $LbL^+[AgNP]_h$ - with 5 bilayers of Chitosan/Alginate with 4mg/mL AgNP, B – uncoated Ti Substrate (Bare). Panels B and C shows Linear regression plots of nanoparticle concentration on antibacterial activity against *S. aureus* cells exposed to nanoparticle-imbedded PEMs.

## 5. Conclusions

This research sought to establish a proof-of-concept for a novel bacteriostatic, bactericidal, and osteoconductive surface coating for use as an anti-infective surface modification and preventative measure against PJI. The LbL technique was used to assemble PEMs with imbedded nanoparticles of titanium dioxide or silver on the titanium substrate featuring both solid and porous matrices. Several surface characterization techniques confirmed that the PEM and its imbedded nanoparticles were successfully deposited on the substrate. The PEM-embeddd $TiO_2$NPs showed superior preosteoblast cell viability even at higher doses of $TiO_2$NPs as well as a promoted osteogenic differentiation of osteoblastic cells compared to PME-embedded AgNPs. The antibacterial activity was found to be similar for PMEs whether $TiO_2$ or AgNPs were imbedded in PMEs. However, a dose-dependent antibacterial activity toward growth inhibition was observed for tested concentrations of $TiO_2$NPs.

Although further in vitro and in vivo studies are necessary to refine the PEM's coating and to perform more quantitative analyses of coating imbedding titanium oxide capabilities and dose-dependent cell viability, proliferation and osteogenic differentiation, the findings reported here are considered a first step toward developing a suitable coating for encapsulation of $TiO_2$ that has the desired antibacterial effect but do not substantially harm the host cell. As a result, such a coating may be an alternative to the use of highly toxic AgNPs for the purposes of infection prevention and enhanced bone growth.

**Supplementary Materials:** not applicable.

**Author Contributions:** Conceptualization, AH, MTan, MTab; methodology MR, NCTD, GM; software, MR; investigation MR, NCTD, MTab, AH; resources, AH, MTab, DN; data curation MR, AH, MT; writing—original draft preparation, MR, NCTD, AH, MTab; writing—review and editing, NCTD, AH, MTab and MTan; supervision, AH, MTab; project administration AH, MTab; funding acquisition AH, MTab. All authors have read and agreed to the published version of the manuscript.

**Funding:** This research received funding MI4 (McGill Interdisciplinary Initiative in Infection and Immunity).

**Institutional Review Board Statement:** not applicable.

**Informed Consent Statement:** not applicable.

**Data Availability Statement:** The data presented in this study are available on request from the corresponding author.

**Acknowledgments:** The authors would like to acknowledge M. Lugnina as well as M. Yitayew the technical advice on nanoparticle encapsulation, MC3T3 cell culture and for multilayer coating.

**Conflicts of Interest:** The authors declare no conflict of interest. The funders don't have any role in the study's design, collection, analysis, or interpretation of data in the writing of the manuscript.

## References

1. Data Quality Documentation for Users: Canadian Joint Replacement Registry, 2020–2021 Data.
2. Lazic, I.; Scheele, C.; Pohlig, F.; von Eisenhart-Rothe, R.; Suren, C. Treatment Options in PJI – Is Two-Stage Still Gold Standard? *J Orthop* **2021**, *23*, 180–184, doi:10.1016/j.jor.2020.12.021.
3. Premkumar, A.; Kolin, D.A.; Farley, K.X.; Wilson, J.M.; McLawhorn, A.S.; Cross, M.B.; Sculco, P.K. Projected Economic Burden of Periprosthetic Joint Infection of the Hip and Knee in the United States. *The Journal of Arthroplasty* **2021**, *36*, 1484-1489.e3, doi:10.1016/j.arth.2020.12.005.
4. Luthringer, T.A.; Fillingham, Y.A.; Okroj, K.; Ward, E.J.; Della Valle, C. Periprosthetic Joint Infection After Hip and Knee Arthroplasty: A Review for Emergency Care Providers. *Annals of Emergency Medicine* **2016**, *68*, 324–334, doi:10.1016/j.annemergmed.2016.03.004.

5. Otto-Lambertz, C.; Yagdiran, A.; Wallscheid, F.; Eysel, P.; Jung, N. Periprosthetic Infection in Joint Replacement. *Dtsch Arztebl Int* **2017**, *114*, 347–353, doi:10.3238/arztebl.2017.0347.
6. Muñoz-Gallego, I.; Meléndez-Carmona, M.Á.; Lora-Tamayo, J.; Garrido-Allepuz, C.; Chaves, F.; Sebastián, V.; Viedma, E. Microbiological and Molecular Features Associated with Persistent and Relapsing Staphylococcus Aureus Prosthetic Joint Infection. *Antibiotics* **2022**, *11*, 1119, doi:10.3390/antibiotics11081119.
7. Patel, R. Periprosthetic Joint Infection. *New England Journal of Medicine* **2023**, *388*, 251–262, doi:10.1056/NEJMra2203477.
8. Rajput, V.; Meek, R.M.D.; Haddad, F.S. Periprosthetic Joint Infection: What Next? *The Bone & Joint Journal* **2022**, *104-B*, 1193–1195, doi:10.1302/0301-620X.104B11.BJJ-2022-0944.
9. Oliveira, W.F.; Silva, P.M.S.; Silva, R.C.S.; Silva, G.M.M.; Machado, G.; Coelho, L.C.B.B.; Correia, M.T.S. Staphylococcus Aureus and Staphylococcus Epidermidis Infections on Implants. *Journal of Hospital Infection* **2018**, *98*, 111–117, doi:10.1016/j.jhin.2017.11.008.
10. Hays, M.R.; Kildow, B.J.; Hartman, C.W.; Lyden, E.R.; Springer, B.D.; Fehring, T.K.; Garvin, K.L. Increased Incidence of Methicillin-Resistant Staphylococcus Aureus in Knee and Hip Prosthetic Joint Infection. *The Journal of Arthroplasty* **2023**, *38*, S326–S330, doi:10.1016/j.arth.2023.02.025.
11. Papadimitriou-Olivgeris, M.; Senn, L.; Bertelli, C.; Grandbastien, B.; Steinmetz, S.; Boillat-Blanco, N. Prevalence and Factors Associated with Prosthetic Joint Infections in Patients with Staphylococcus Aureus Bacteraemia: A 7-Year Retrospective Study. *Antibiotics* **2022**, *11*, 1323, doi:10.3390/antibiotics11101323.
12. Missiakas, D.M.; Schneewind, O. Growth and Laboratory Maintenance of Staphylococcus Aureus. *Current Protocols in Microbiology* **2013**, *28*, 9C.1.1-9C.1.9, doi:10.1002/9780471729259.mc09c01s28.
13. Rao, Y.; Peng, H.; Shang, W.; Hu, Z.; Yang, Y.; Tan, L.; Li, M.; Zhou, R.; Rao, X. A Vancomycin Resistance-Associated WalK(S221P) Mutation Attenuates the Virulence of Vancomycin-Intermediate Staphylococcus Aureus. *Journal of Advanced Research* **2022**, *40*, 167–178, doi:10.1016/j.jare.2021.11.015.
14. Nikolic, P.; Mudgil, P. The Cell Wall, Cell Membrane and Virulence Factors of Staphylococcus Aureus and Their Role in Antibiotic Resistance. *Microorganisms* **2023**, *11*, 259, doi:10.3390/microorganisms11020259.
15. Mahfouz, A.A.; Said, H.S.; Elfeky, S.M.; Shaaban, M.I. Inhibition of Erythromycin and Erythromycin-Induced Resistance among Staphylococcus Aureus Clinical Isolates. *Antibiotics* **2023**, *12*, 503, doi:10.3390/antibiotics12030503.
16. Kunutsor, S.K.; Beswick, A.D.; Whitehouse, M.R.; Wylde, V.; Blom, A.W. Debridement, Antibiotics and Implant Retention for Periprosthetic Joint Infections: A Systematic Review and Meta-Analysis of Treatment Outcomes. *Journal of Infection* **2018**, *77*, 479–488, doi:10.1016/j.jinf.2018.08.017.
17. Gramlich, Y.; Parvizi, J. Enough Is Enough: Salvage Procedures in Severe Periprosthetic Joint Infection. *Arthroplasty* **2023**, *5*, 36, doi:10.1186/s42836-023-00182-7.
18. Liukkonen, R.; Honkanen, M.; Skyttä, E.; Eskelinen, A.; Karppelin, M.; Reito, A. Clinical Outcomes After Revision Hip Arthroplasty Due to Prosthetic Joint Infection—A Single-Center Study of 369 Hips at a High-Volume Center With a Minimum of One Year Follow-Up. *The Journal of Arthroplasty* **2023**, doi:10.1016/j.arth.2023.08.078.
19. Olearo, F.; Zanichelli, V.; Exarchakou, A.; Both, A.; Uçkay, I.; Aepfelbacher, M.; Rohde, H. The Impact of Antimicrobial Therapy Duration in the Treatment of Prosthetic Joint Infections Depending on Surgical Strategies: A Systematic Review and Meta-Analysis. *Open Forum Infectious Diseases* **2023**, *10*, ofad246, doi:10.1093/ofid/ofad246.
20. Le Vavasseur, B.; Zeller, V. Antibiotic Therapy for Prosthetic Joint Infections: An Overview. *Antibiotics* **2022**, *11*, 486, doi:10.3390/antibiotics11040486.
21. Shabana, N.S.; Seeber, G.; Soriano, A.; Jutte, P.C.; Westermann, S.; Mithoe, G.; Pirii, L.; Siebers, T.; Have, B. ten; Zijlstra, W.; et al. The Clinical Outcome of Early Periprosthetic Joint Infections Caused by Staphylococcus Epidermidis and Managed by Surgical Debridement in an Era of Increasing Resistance. *Antibiotics* **2023**, *12*, 40, doi:10.3390/antibiotics12010040.
22. Chouirfa, H.; Bouloussa, H.; Migonney, V.; Falentin-Daudré, C. Review of Titanium Surface Modification Techniques and Coatings for Antibacterial Applications. *Acta Biomaterialia* **2019**, *83*, 37–54, doi:10.1016/j.actbio.2018.10.036.
23. Dadi, N.C.T.; Bujdák, J.; Medvecká, V.; Pálková, H.; Barlog, M.; Bujdáková, H. Surface Characterization and Anti-Biofilm Effectiveness of Hybrid Films of Polyurethane Functionalized with Saponite and Phloxine B. *Materials* **2021**, *14*, 7583, doi:10.3390/ma14247583.
24. Dadi, N.C. teja; Dohál, M.; Medvecká, V.; Bujdák, J.; Koči, K.; Zahoranová, A.; Bujdáková, H. Physico-Chemical Characterization and Antimicrobial Properties of Hybrid Film Based on Saponite and Phloxine B. *Molecules* **2021**, *26*, 325, doi:10.3390/molecules26020325.

25. Birkett, M.; Zia, A.W.; Devarajan, D.K.; Soni; Panayiotidis, M.I.; Joyce, T.J.; Tambuwala, M.M.; Serrano-Aroca, Á. Multi-Functional Bioactive Silver- and Copper-Doped Diamond-like Carbon Coatings for Medical Implants. *Acta Biomaterialia* **2023**, *167*, 54–68, doi:10.1016/j.actbio.2023.06.037.
26. Xie, H.; Liu, Y.; An, H.; Yi, J.; Li, C.; Wang, X.; Chai, W. Recent Advances in Prevention, Detection and Treatment in Prosthetic Joint Infections of Bioactive Materials. *Frontiers in Bioengineering and Biotechnology* **2022**, *10*.
27. Piñera-Avellaneda, D.; Buxadera-Palomero, J.; Ginebra, M.-P.; Calero, J.A.; Manero, J.M.; Rupérez, E. Surface Competition between Osteoblasts and Bacteria on Silver-Doped Bioactive Titanium Implant. *Biomaterials Advances* **2023**, *146*, 213311, doi:10.1016/j.bioadv.2023.213311.
28. Elizarova, I.S.; Luckham, P.F. Layer-by-Layer Adsorption: Factors Affecting the Choice of Substrates and Polymers. *Advances in Colloid and Interface Science* **2018**, *262*, 1–20, doi:10.1016/j.cis.2018.11.003.
29. Almeida, A.C.; Vale, A.C.; Pires, R.A.; Reis, R.L.; Alves, N.M. Layer-by-Layer Films Based on Catechol-Modified Polysaccharides Produced by Dip- and Spin-Coating onto Different Substrates. *Journal of Biomedical Materials Research Part B: Applied Biomaterials* **2020**, *108*, 1412–1427, doi:10.1002/jbm.b.34489.
30. Zhong, X.; Song, Y.; Yang, P.; Wang, Y.; Jiang, S.; Zhang, X.; Li, C. Titanium Surface Priming with Phase-Transited Lysozyme to Establish a Silver Nanoparticle-Loaded Chitosan/Hyaluronic Acid Antibacterial Multilayer via Layer-by-Layer Self-Assembly. *PLOS ONE* **2016**, *11*, e0146957, doi:10.1371/journal.pone.0146957.
31. Venkatesan, J.; Kim, S.-K. Chitosan Composites for Bone Tissue Engineering—An Overview. *Marine Drugs* **2010**, *8*, 2252–2266, doi:10.3390/md8082252.
32. Venkatesan, J.; Bhatnagar, I.; Manivasagan, P.; Kang, K.-H.; Kim, S.-K. Alginate Composites for Bone Tissue Engineering: A Review. *International Journal of Biological Macromolecules* **2015**, *72*, 269–281, doi:10.1016/j.ijbiomac.2014.07.008.
33. Thambirajoo, M.; Maarof, M.; Lokanathan, Y.; Katas, H.; Ghazalli, N.F.; Tabata, Y.; Fauzi, M.B. Potential of Nanoparticles Integrated with Antibacterial Properties in Preventing Biofilm and Antibiotic Resistance. *Antibiotics* **2021**, *10*, 1338, doi:10.3390/antibiotics10111338.
34. Wang, L.; Hu, C.; Shao, L. The Antimicrobial Activity of Nanoparticles: Present Situation and Prospects for the Future. *International Journal of Nanomedicine* **2017**, *12*, 1227–1249, doi:10.2147/IJN.S121956.
35. Qing, Y.; Cheng, L.; Li, R.; Liu, G.; Zhang, Y.; Tang, X.; Wang, J.; Liu, H.; Qin, Y. Potential Antibacterial Mechanism of Silver Nanoparticles and the Optimization of Orthopedic Implants by Advanced Modification Technologies. *International Journal of Nanomedicine* **2018**, *13*, 3311–3327, doi:10.2147/IJN.S165125.
36. Abo-zeid, Y.; Williams, G.R. The Potential Anti-Infective Applications of Metal Oxide Nanoparticles: A Systematic Review. *WIREs Nanomedicine and Nanobiotechnology* **2020**, *12*, e1592, doi:10.1002/wnan.1592.
37. Sharma, V.K.; Siskova, K.M.; Zboril, R.; Gardea-Torresdey, J.L. Organic-Coated Silver Nanoparticles in Biological and Environmental Conditions: Fate, Stability and Toxicity. *Advances in Colloid and Interface Science* **2014**, *204*, 15–34, doi:10.1016/j.cis.2013.12.002.
38. Lojk, J.; Repas, J.; Veranič, P.; Bregar, V.B.; Pavlin, M. Toxicity Mechanisms of Selected Engineered Nanoparticles on Human Neural Cells in Vitro. *Toxicology* **2020**, *432*, 152364, doi:10.1016/j.tox.2020.152364.
39. Xu, L.; Wang, Y.-Y.; Huang, J.; Chen, C.-Y.; Wang, Z.-X.; Xie, H. Silver Nanoparticles: Synthesis, Medical Applications and Biosafety. *Theranostics* **2020**, *10*, 8996–9031, doi:10.7150/thno.45413.
40. Kuppusamy, P.; Kim, S.; Kim, S.-J.; Song, K.-D. Antimicrobial and Cytotoxicity Properties of Biosynthesized Gold and Silver Nanoparticles Using D. Brittonii Aqueous Extract. *Arabian Journal of Chemistry* **2022**, *15*, 104217, doi:10.1016/j.arabjc.2022.104217.
41. Chauhan, V.; Dhiman, V.K.; Mahajan, G.; Pandey, A.; Kanwar, S.S. Synthesis and Characterization of Silver Nanoparticles Developed Using a Novel Lipopeptide(s) Biosurfactant and Evaluating Its Antimicrobial and Cytotoxic Efficacy. *Process Biochemistry* **2023**, *124*, 51–62, doi:10.1016/j.procbio.2022.11.002.
42. Mouriya, G.K.; Mohammed, M.; Azmi, A.A.; Khairul, W.M.; Karunakaran, T.; Amirul, A.-A.A.; Ramakrishna, S.; Santhanam, R.; Vigneswari, S. Green Synthesis of Cicer Arietinum Waste Derived Silver Nanoparticle for Antimicrobial and Cytotoxicity Properties. *Biocatalysis and Agricultural Biotechnology* **2023**, *47*, 102573, doi:10.1016/j.bcab.2022.102573.
43. Poon, W.-L.; Alenius, H.; Ndika, J.; Fortino, V.; Kolhinen, V.; Meščeriakovas, A.; Wang, M.; Greco, D.; Lähde, A.; Jokiniemi, J.; et al. Nano-Sized Zinc Oxide and Silver, but Not Titanium Dioxide, Induce Innate and Adaptive Immunity and Antiviral Response in Differentiated THP-1 Cells. *Nanotoxicology* **2017**, *11*, 936–951, doi:10.1080/17435390.2017.1382600.
44. Poon, W.-L.; Lee, J.C.-Y.; Leung, K.S.; Alenius, H.; El-Nezami, H.; Karisola, P. Nanosized Silver, but Not Titanium Dioxide or Zinc Oxide, Enhances Oxidative Stress and Inflammatory Response by Inducing 5-HETE Activation in THP-1 Cells. *Nanotoxicology* **2020**, *14*, 453–467, doi:10.1080/17435390.2019.1687776.

45. Zheng, H.; He, S.; Zhou, L.; Yuan, J.; Jiang, B.; Ni, X.; Lu, K.; Zhang, P.; Zhao, Q. A Cytocompatible Microporous Sr-Doped Titanium Dioxide Coating Fabricated by Plasma Electrolytic Oxidation. *Frontiers in Materials* **2023**, *10*.
46. Hari Raj, K.; Gnanavel, S.; Ramalingam, S. Investigation of 3D Printed Biodegradable PLA Orthopedic Screw and Surface Modified with Nanocomposites (Ti–Zr) for Biocompatibility. *Ceramics International* **2023**, *49*, 7299–7307, doi:10.1016/j.ceramint.2022.10.188.
47. Noreen, S.; Wang, E.; Feng, H.; Li, Z. Functionalization of TiO2 for Better Performance as Orthopedic Implants. *Materials* **2022**, *15*, 6868, doi:10.3390/ma15196868.
48. Rahnamaee, S.Y.; Dehnavi, S.M.; Bagheri, R.; Barjasteh, M.; Golizadeh, M.; Zamani, H.; Karimi, A. Boosting Bone Cell Growth Using Nanofibrous Carboxymethylated Cellulose and Chitosan on Titanium Dioxide Nanotube Array with Dual Surface Charges as a Novel Multifunctional Bioimplant Surface. *International Journal of Biological Macromolecules* **2023**, *228*, 570–581, doi:10.1016/j.ijbiomac.2022.12.159.
49. D'Agostino, A.; Bertolini, M.; Bono, N.; Pavarini, M.; Tarsini, P.; Candiani, G.; De Nardo, L.; Chiesa, R. Antibacterial Titanium Dioxide Coatings for CoCrMo Orthopaedic Implants. *Applied Surface Science* **2023**, *609*, 155300, doi:10.1016/j.apsusc.2022.155300.
50. Popova, A.D.; Sheveyko, A.N.; Kuptsov, K.A.; Advakhova, D.Yu.; Karyagina, A.S.; Gromov, A.V.; Krivozubov, M.S.; Orlova, P.A.; Volkov, A.V.; Slukin, P.V.; et al. Osteoconductive, Osteogenic, and Antipathogenic Plasma Electrolytic Oxidation Coatings on Titanium Implants with BMP-2. *ACS Appl. Mater. Interfaces* **2023**, *15*, 37274–37289, doi:10.1021/acsami.3c08954.
51. Bélteky, P.; Rónavári, A.; Zakupszky, D.; Boka, E.; Igaz, N.; Szerencsés, B.; Pfeiffer, I.; Vágvölgyi, C.; Kiricsi, M.; Kónya, Z. Are Smaller Nanoparticles Always Better? Understanding the Biological Effect of Size-Dependent Silver Nanoparticle Aggregation Under Biorelevant Conditions. *International Journal of Nanomedicine* **2021**, *16*, 3021–3040, doi:10.2147/IJN.S304138.
52. Martin, H.J.; Schulz, K.H.; Bumgardner, J.D.; Walters, K.B. XPS Study on the Use of 3-Aminopropyltriethoxysilane to Bond Chitosan to a Titanium Surface. *Langmuir* **2007**, *23*, 6645–6651, doi:10.1021/la063284v.
53. Holmes, C.A.; Tabrizian, M. Enhanced MC3T3 Preosteoblast Viability and Adhesion on Polyelectrolyte Multilayer Films Composed of Glycol-Modified Chitosan and Hyaluronic Acid. *Journal of Biomedical Materials Research Part A* **2012**, *100A*, 518–526, doi:10.1002/jbm.a.33305.
54. Nayef, L.; Castiello, R.; Tabrizian, M. Washless Method Enables Multilayer Coating of an Aggregation-Prone Nanoparticulate Drug Delivery System with Enhanced Yields, Colloidal Stability, and Scalability. *Macromolecular Bioscience* **2017**, *17*, 1600535, doi:10.1002/mabi.201600535.
55. Bernards, D.A.; Desai, T.A. Nanoscale porosity in polymer films: fabrication and therapeutic applications. *Soft Matter*. **2010**, 6(8), 1621-1631. doi: 10.1039/B922303G.
56. Yan, L.; Yergeshov, A.A.; Al-Thaher, Y.; Avdokushina, S.; Statsenko, E.; Abdullin, T.I.; Prokopovich, P. Nanocomposite orthopaedic bone cement combining long-acting dual antimicrobial drugs. Biomaterials Advances, **2023**,153, 213538. doi.org/10.1016/j.bioadv.2023.213538.
57. Misra, R.D.K.; Thein-Han, W.W.; Pesacreta, T.C.; Somani, M.C.; Karjalainen, L.P. Biological Significance of Nanograined/Ultrafine-Grained Structures: Interaction with Fibroblasts. *Acta Biomaterialia* **2010**, *6*, 3339–3348, doi:10.1016/j.actbio.2010.01.034.
58. Yazid, M.D.; Ariffin, S.H.Z.; Senafi, S.; Razak, M.A.; Wahab, R.M.A. Determination of the Differentiation Capacities of Murines' Primary Mononucleated Cells and MC3T3-E1 Cells. *Cancer Cell International* **2010**, *10*, 42, doi:10.1186/1475-2867-10-42.
59. Nie, W.; Peng, C.; Zhou, X.; Chen, L.; Wang, W.; Zhang, Y.; Ma, P.X.; He, C. Three-Dimensional Porous Scaffold by Self-Assembly of Reduced Graphene Oxide and Nano-Hydroxyapatite Composites for Bone Tissue Engineering. *Carbon* **2017**, *116*, 325–337, doi:10.1016/j.carbon.2017.02.013.
60. Metwally, S.; Stachewicz, U. Surface Potential and Charges Impact on Cell Responses on Biomaterials Interfaces for Medical Applications. *Materials Science and Engineering: C* **2019**, *104*, 109883, doi:10.1016/j.msec.2019.109883.
61. Zheng, S.; Bawazir, M.; Dhall, A.; Kim, H.-E.; He, L.; Heo, J.; Hwang, G. Implication of Surface Properties, Bacterial Motility, and Hydrodynamic Conditions on Bacterial Surface Sensing and Their Initial Adhesion. *Frontiers in Bioengineering and Biotechnology* **2021**, *9*.
62. Shen, J.; Gao, P.; Han, S.; Kao, R.Y.T.; Wu, S.; Liu, X.; Qian, S.; Chu, P.K.; Cheung, K.M.C.; Yeung, K.W.K. A Tailored Positively-Charged Hydrophobic Surface Reduces the Risk of Implant Associated Infections. *Acta Biomaterialia* **2020**, *114*, 421–430, doi:10.1016/j.actbio.2020.07.040.
63. Lv, H.; Chen, Z.; Yang, X.; Cen, L.; Zhang, X.; Gao, P. Layer-by-Layer Self-Assembly of Minocycline-Loaded Chitosan/Alginate Multilayer on Titanium Substrates to Inhibit Biofilm Formation. *J Dent* **2014**, *42*, 1464–1472, doi:10.1016/j.jdent.2014.06.003.

64. Rodríguez López, A. de L.; Lee, M.-R.; Ortiz, B.J.; Gastfriend, B.D.; Whitehead, R.; Lynn, D.M.; Palecek, S.P. Preventing S. Aureus Biofilm Formation on Titanium Surfaces by the Release of Antimicrobial β-Peptides from Polyelectrolyte Multilayers. *Acta Biomater* **2019**, *93*, 50–62, doi:10.1016/j.actbio.2019.02.047.
65. Archana, D.; Dutta, J.; Dutta, P.K. Evaluation of Chitosan Nano Dressing for Wound Healing: Characterization, in Vitro and in Vivo Studies. *International Journal of Biological Macromolecules* **2013**, *57*, 193–203, doi:10.1016/j.ijbiomac.2013.03.002.